Research Article

Naushad Ahmad*, Manawwer Alam, Rizwan Wahab, Mukhtar Ahmed, Ashfaq Ahmad

Synthesis, spectral and thermo-kinetics explorations of Schiff-base derived metal complexes

https://doi.org/10.1515/chem-2020-0168
received March 17, 2020; accepted August 25, 2020

Abstract: Schiff-base ligand, 2,6-bis(benzimino)-4-phenyl-1,3,5-triazine (L), and its transition metal complexes of Co(II), Ni(II), and Cu(II) were synthesized by refluxing the reaction mixture and its analytical, spectral, and thermogravimetric characteristics were explored by various techniques: AAS, FT-IR, UV-vis, TG-DTG, CHNS/O, and VSM. It was observed that all the metal containing complexes are non-electrolytic, mononuclear, and paramagnetic in nature, confirmed by the molar conductance and magnetic susceptibility measurements. Optical spectral data were used to investigate the geometrical and spectral parameters of $[Co(L)(ac)_2]$, $[Ni(L)(ac)_2]$, $[Cu(L)(ac)_2]$, $[Cu(L)(acac)_2]$, and $[Cu(L)(fmc)_2]$ complexes. Simultaneous thermal analyses (TG-DTG) in nitrogen atmosphere reveal that the ligand decomposes in one step, $[Co(L)(ac)_2]$, $[Ni(L)(ac)_2]$, and $[Cu(L)(ac)_2]$ complexes are decomposed in three steps, whereas $[Cu(L)(acac)_2]$ and $[Cu(L)(fmc)_2]$ are decomposed in five and two steps, respectively. In addition, activation energy (E_a) and pre-exponential factor ($\ln A$) were evaluated by TG-DTG decomposition steps of compounds using the Coats–Redfern formula. Enthalpy (ΔH), entropy (ΔS), and Gibbs free energy (ΔG) of the as-prepared metal complexes were also speculated by various thermodynamic equations.

Keywords: Schiff-base, metal complexes, spectroscopic, kinetics, Coats–Redfern.

1 Introduction

Schiff base is one of the important classes of ligands, which have attracted special interest and are fast developing on account of their industrial, thermal, and biological applications. It is well documented that the combination of metal ions with Schiff bases provides flexible binding sites, which lead to materials with interesting properties such as reversibly binding oxygen capacity, catalytic conversion reaction: hydrogenation of olefins, transfer of the amino group, photochromic, sensing, magnetic, and optical properties [1–6]. Transition metal complexes of Schiff bases, fabricated from aldehydes and amines, have been widely explored. Because of the presence of both nitrogen and oxygen donor atoms in the Schiff base, they can easily coordinate with transition metal ions, producing enhanced thermally stable and colored metal complexes. They can serve as models of biologically important species and find applications in biomimetic catalytic reactions, materials chemistry and have a strong anticancer activity [7,8].

With the advancement of science and explosion of technologies, researchers have been showing an increasing interest in solid-state thermal kinetic studies of transition metal complexes containing both nitrogen and oxygen donor ligands [9,10]. Various thermal analysis techniques, such as thermogravimetric analysis (TGA), derivative thermogravimetry (DTG), differential scanning calorimetry (DSC), and differential thermal analysis (DTA), were extensively applied to investigate the thermal behavior of Schiff-base metal complexes such as activation energy, pre-exponential factor, and reaction order [11–13]. Among them, the TG-DTG technique is widely applied because of its simplicity and the information afforded by simple thermograms. On

* **Corresponding author: Naushad Ahmad,** Department of Chemistry, College of Science, King Saud University, P.O. Box 2455, Riyadh-11451, Kingdom of Saudi Arabia,
e-mail: anaushad@ksu.edu.sa
Manawwer Alam, Ashfaq Ahmad: Department of Chemistry, College of Science, King Saud University, P.O. Box 2455, Riyadh-11451, Kingdom of Saudi Arabia
Rizwan Wahab, Mukhtar Ahmed: Department of Zoology, College of Science, King Saud University, P.O. Box 2455, Riyadh-11451, Kingdom of Saudi Arabia

thermal treatment, these complexes undergo decomposition reactions and release heat, gaseous products, and solid metal oxide residues, which could be used in explosives, propellants, pyrotechnic compositions, and preparation of environmental sensors for the detection of trace-level different hazardous materials [14–16].

Thus, in the light of the above enormous applications, in the present manuscript, we discussed the synthesis, structural features, and kinetic parameters of the Schiff base derived from 2-pyridinecarboxaldehyde and 2,6-diamino-4-phenyl-1,3,5-triazine and its Co(II), Ni(II), and Cu(II) acetates as well as acetylacetonate and trifluoromethanesulfonate Cu(II) complexes. In the kinetic study on thermal decomposition, the Coats–Redfern equation is used for the calculation of kinetic parameters such as activation energy (E), enthalpy (ΔH), entropy (ΔS), and Gibbs free energy (ΔG).

2 Experimental

2.1 Materials

2-Pyridinecarboxaldehyde, 2,6-diamino-4-phenyl-1,3,5-triazine, copper(II) acetylacetonate [$Cu(C_5H_7O_2)_2$], copper(II) trifluoromethanesulfonate [$(CF_3SO_3)_2Cu$], copper(II) acetate monohydrate [$(CH_3COO)_2Cu{\cdot}H_2O$], cobalt(II) acetate tetrahydrate [$(CH_3COO)_2Co{\cdot}4H_2O$], and nickel(II) acetate hydrate [$(CH_3COO)_2Ni{\cdot}H_2O$] reagent grades were purchased from Sigma-Aldrich. Solvents, such as dimethylformamide (DMF), dimethyl sulfoxide (DMSO), ethanol, methanol, diethyl ether, and acetone for synthesis and physical measurements, were obtained from Fluka and used without further purification.

2.2 Physical measurements

Elemental analyses of fabricated samples in powder form were performed on PerkinElmer 2400 Series II CHNS/O Elemental Analyzer. For the determination of metal percentages, atomic absorption spectroscopy (AAS), PerkinElmer 1100B spectrometer, was used after microwave digestion (TOPwave Analytik Jena microwave) of samples in the mixture of 65% HNO_3 and 37% HCl. The FT-IR spectra were used for the determination of functional groups using the KBr disk method in the 4,000–400 cm^{-1} region on a Bruker Tensor 27 FT-IR spectrophotometer at room temperature. The electronic spectra of fabricated samples in DMF solution were recorded at room temperature on a UV-2550 spectrophotometer (Shimadzu, Japan). The ^1H NMR spectrum of the Schiff-base ligand was recorded on a JEOL-GSX 300-MHz FX-1000 FT-NMR at room temperature using deuterated DMSO-d_6 as a solvent and TMS as an internal standard. Chemical shifts are given in ppm, relative to TMS. Simultaneous TG-DTG of samples was carried out by SDT-Q600 (TA Instrument) in nitrogen atmosphere (100 mL min^{-1}) at a heating rate of 20°C min^{-1} in the temperature range from room temperature to 800°C.

2.3 Synthesis of ligand [2,6-bis (benzimino)-4-phenyl-1,3,5-triazine]

A hot methanol solution of 2,6-diamino-4-phenyl-1,3,5-triazine (1.8 g, 0.01 mol) was added dropwise to a hot methanol solution of 2-pyridinecarboxaldehyde (2.14 g, 0.02 mol) and the reaction mixture was refluxed at 70°C for 6 h. The course of reaction was monitored by thin-layer chromatography (TLC). After completing the reaction, the reaction mixture was left to stand overnight. The resulted brown colored solid was filtered off, washed with ether and acetone, and dried under vacuum. The product is soluble in DMF and DMSO and insoluble in MeOH, EtOH, $CHCl_3$, acetone, and benzene.

2.4 Synthesis of Co(II), Ni(II), and Cu(II) complexes

A hot methanol solution of 2,6-diamino-4-phenyl-1,3,5-triazine (1.8 g, 0.01 mol) was added dropwise to a hot methanol solution of 2-pyridinecarboxaldehyde (2.14 g, 0.02 mol) to form a brown suspension. Then an appropriate amount of Co(II), Ni(II), and Cu(II) (0.01 mol) metal salts was added, refluxed at 70°C for 4 h, and left to stand overnight at room temperature. The obtained complexes were filtered off, washed several times with cold EtOH, water, and ether, and then dried under vacuum.

Ethical approval: The conducted research is not related to either human or animal use.

3 Results and discussions

Synthetic pathways for the preparation of ligand and its metal complexes are shown in Scheme 1. The Schiff-base derived Co(II), Ni(II), and Cu(II) metal complexes are stable at room temperature and soluble in DMF, DMSO, THF, and $CHCl_3$. The formation of products was recognized by FT-IR, NMR, UV-vis, AAS, and elemental analyses. Physical characterization, molar conductance, and elemental analyses of ligand and its metal complexes are listed in Table 1. The stoichiometry of ligand and its metal complexes was confirmed by their elemental analyses. The analytical data of metal complexes correspond with the general formula MLX_2, where L = ligand; M = Co(II), Ni(II), or Cu(II); and X = acetate, acetylacetonate, and trifluoromethanesulfonate ions. The observed molar conductance measured in DMF solution is 8.90–10.50 $\Omega^{-1}\,cm^2\,mol^{-1}$ and thereby indicates that all complexes are non-electrolytic and mononuclear in nature [16,17].

3.1 FT-IR study

The FT-IR spectral data containing relevant characteristic band regions of the ligand and its metal complexes are registered in Table 2. The ligand formation has been confirmed by the appearance of an azomethine ν(C═N^a) band at 1,630 cm^{-1} and the absence of a $\nu(NH_2)$ band at 3,400 cm^{-1} indicates that the Schiff-base condensation occurred between carbonyl groups of 2-pyridinecarboxaldehyde and amino groups of 2,6-diamino-4-phenyl-1,3,5-triazine [18,19]. The vibrations of 2-pyridinecarboxaldehyde ν(C═N^b) and 2,6-diamino-4-phenyl-1,3,5-triazine ν(C═N^c) groups of ligands are dictated at 1,558 and 1,605 cm^{-1}, respectively. The spectrum of the ligand is also characterized by two medium bands at 608 and 413 cm^{-1}, which are considered "in plane" and "out plane" deformation modes of 2-pyridinecarboxaldehyde rings, respectively [18]. A major negative shift in the ν(C═N^a) band, which appeared in the 1,610–1,585 cm^{-1} region for complexes as compared to the ligand, endows that two azomethine nitrogens are coordinated with metal ions. Moreover, distinct bands in the far-IR region at 455–410 cm^{-1} were assigned the ν(M–N) band [20], which provides a direct evidence for the coordinated metal ion in the ligand frame. Co(II) and Ni(II) complexes have also shown negative shifts in the ν(C═N^b) band, which appeared at 1,543 and 1,545 cm^{-1}, respectively, as compared to the ligand, suggesting that 2-pyridinecarboxaldehyde nitrogen is intricate in the coordination with metal ions. The two bands at 1,594–1,579 cm^{-1} and 1,378–1,367 cm^{-1} are assigned asymmetric and symmetric vibrations of acetate ions. The observed bands in these regions indicate that acetate groups are bonded to metal ions in a monodentate manner in case of $[CuL(ac)_2]$, $[NiL(ac)_2]$, and $[CoL(ac)_2]$ [21]. The bands in $[CuL(acac)_2]$ observed at 1,565 and 1,380 cm^{-1} regions, ascribed to ν_{as}(C–O) and ν_s(C–O) modes of coordinated acetylacetonate molecules, suggest that acetylacetonate ions are retained in the complex [22]. The vibrations of the triflate anion in $[CuL(fms)_2]$ are observed at 1,275, 1,035 ν_{as}(S═O), and (S═O); 1,220, 1,160ν_s(C–F), and ν_{as}(C–F) cm^{-1} are in agreement with the previous literature on monodentate coordination [23]. The other absorption bands corresponding to the aromatic ν(C═C), ν(C–H) and aliphatic ν(C–H) appeared at their proper positions. Thus, the FT-IR result indicates that the Schiff-base ligand in complexes is binding through azomethine and 2-pyridinecarboxaldehyde.

3.2 NMR study

To determine the structure of a ligand, the ^{1}HNMR spectrum of the ligand was performed in DMSO-d_6. It did not show any signal corresponding to the primary amine group and aldehyde protons. The singlet peak at 7.49 was assigned to two N═C**H**^{a} protons [24] and doublets at 8.36 to two N═C**H**^{b} protons. The aromatic proton appears at 6.70, 6.87, and 7.48 ppm. The ^{13}C NMR spectral data of the ligand confirm the ^{1}H NMR spectral results. The peaks at 161.2, 153.5, and 157.2 ppm for (**C**═N^a), (**C**═N^b), and (**C**═N^c) are observed. The aromatic ring carbon appears at 130.0, 128.1, 126.3 ppm and other 2-pyridinecarboxaldehyde and 2,6-diamino-4-phenyl-1,3,5-triazine carbon at 120.4, 137.1, 119.0, 146.2 and 161.2, 159.0, 77.3 ppm. Spectral analysis confirmed the formation of a Schiff-base condensation reaction between carbonyl groups of 2-pyridinecarboxaldehyde and amino groups of 2,6-diamino-4-phenyl-1,3,5-triazine.

3.3 UV-visible absorption spectral and magnetic measurements

The spectral parameters calculated by the Tanabe–Sugano diagram, band positions of absorption maxima, band assignments, and proposed geometry are listed in Table 3. The electronic spectrum of the ligand

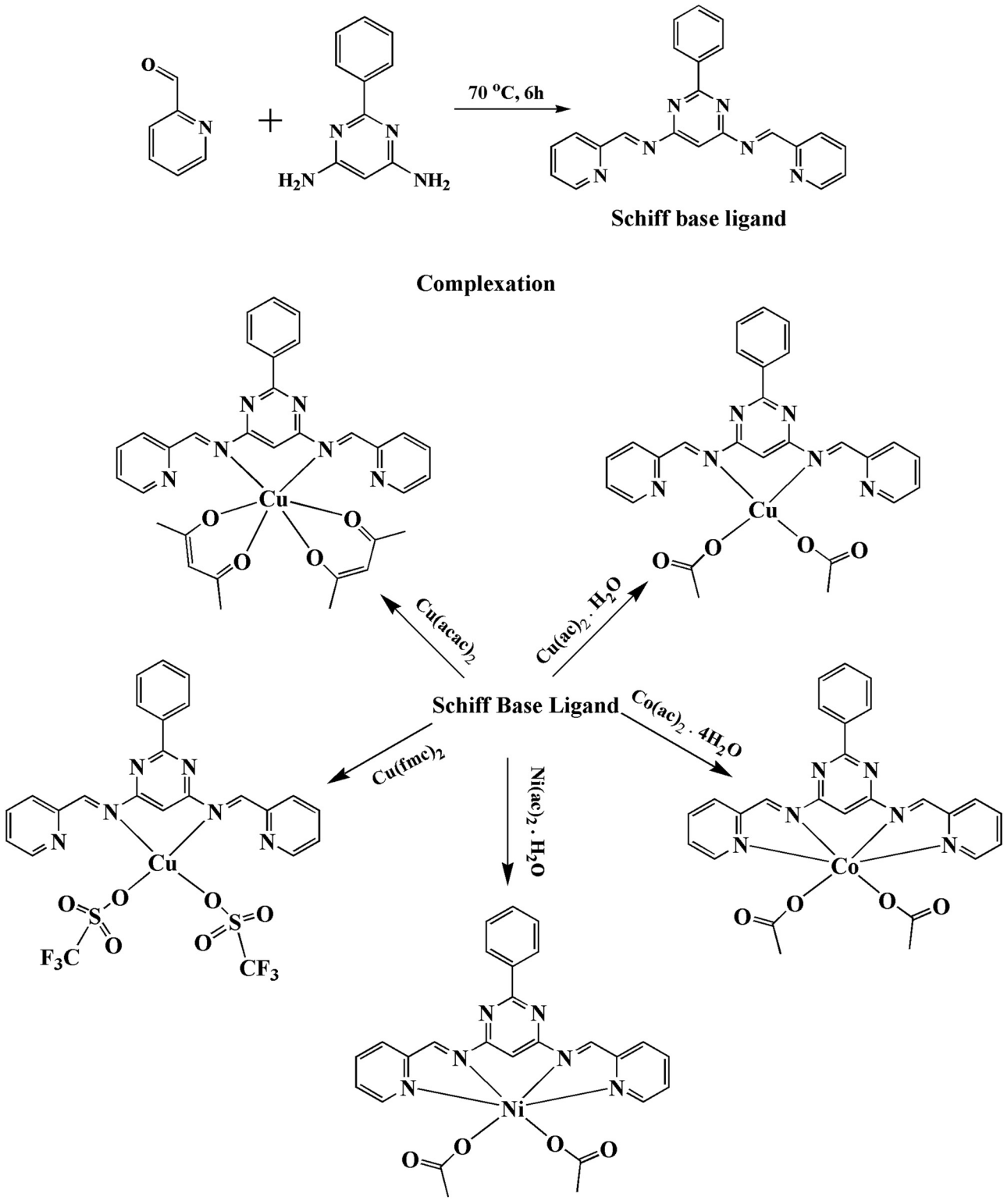

Scheme 1: Schematic preparation of the ligand and its metal complexes.

exhibits a band at 38,461 cm^{-1}, which is allocated π–π*transition of the aromatic ring and shows another broad band at 26,315 cm^{-1}, which is assigned n–π*/π–π* transition of the azomethine group. The hyperchromic shift in metal complex spectra clearly confirmed the coordination of ligand toward metal ions.

Table 1: Analytical and physical data of the Schiff base and its metal complexes

Compound	M.W.	Color	State	M.P.	Yield	Found (calculated) (%)					Molar conductance ($\Omega^{-1}\,cm^2\,mol^{-1}$)
						C	H	N	O	M	
L	365.39	Brown	Liquid	160	65	70.31 (69.03)	4.88 (4.14)	27.08			
$C_{21}H_{15}N_7$								−26.83			
$[CoL(ac)_2]$	542.41	Brown	Solid	315	64	55.3	3.87	18.07	11.79	10.85	8.9
$C_{25}H_{21}N_7O_4Co$						−55.36	−3.9	−18.08	−11.8	−10.87	
$[NiL(ac)_2]$	542.17	Dark	Solid	350	59	55.33	3.87	18.07	11.8	10.86	7.5
$C_{25}H_{21}N_7O_4Ni$		green				−55.38	−3.9	−18.08	−11.8	−10.83	
$[CuL(ac)_2]$	547.02	Green	Solid	310	62	54.84	3.83	17.91	11.69	11.61	6.75
$C_{25}H_{21}N_7O_4Cu$						−54.89	−3.87	−17.92	−11.7	−11.62	
$[CuL(acac)_2]$	659.15	Green	Solid	325	55	56.43	4.39	14.86	14.56	9.63	6.15
$C_{31}H_{29}N_7O_6Cu$						−56.49	−4.43	−14.87	−14.56	−9.94	
$[CuL(fmc)_2]$	642.95	Green	Solid	335	58	44.79	2.33	15.24	9.95	9.88	7.95
$C_{24}H_{15}N_7O_4F_6Cu$						−44.83	−2.35	−15.25	−9.95	−9.88	

The electronic spectrum of the Co(II) metal complex showed two bands at 16,077 and 34,482 cm^{-1} regions assignable to $^4T_{1g}(F) \rightarrow {}^4A_{2g}(F)(\nu_2)$ and $^4T_{1g}(F) \rightarrow 4T_{1g}(P)$ (ν_3) transitions, respectively, which suggest an octahedral geometry around the Co(II) ion (Figure 1a) [25]. On the basis of these assignments, the ligand field parameters calculated for the Co(II) complex are Δ_o = 12098.1 cm^{-1}, B = 864.15 cm^{-1}, and β = 0.771. Similarly, the Ni(II) spectrum revealed an octahedral geometry, which has been confirmed by the electronic transitions at 15,015 and 32,258 cm^{-1}, which represent two $^3A_{2g}(F) \rightarrow {}^3T_{1g}(F)(\nu_2)$ and $^3A_{2g}(F) \rightarrow {}^3T_{1g}(P)(\nu_3)$ transitions, respectively (Figure 1b) [25]. The calculated spectral parameters are as follows: Δ_o = 6606.6 cm^{-1}, B = 600.6 cm^{-1}, and β = 0.556. In the electronic spectra of both the Co(II) and Ni(II) complexes, the first transition was not perceived due to being beyond the range of the used instrument which could have occurred in the near-IR region. Therefore, the reduced Racah parameter from the free ion and β values specified the covalent character of the metal-to-ligand σ bond. The observed magnetic moments 3.75 and 2.76 B.M. for Co(II) and Ni(II) complexes, respectively, pointed out the three and two unpaired electrons for Co(II) and Ni(II), respectively,

Table 2: Infrared spectral data of the ligand and its complexes.

Compound	ν(C=N)	$\nu_{asym}(COO^-)$	ν_{sym} (COO^-)	$\nu(C{=}C)_{arom}$	$\nu(C{-}H)_{arom}$	$\nu(C{-}H)_{ali}$	ν(M–N)	ν(M–O)
L	1,630[a] 1,558[b] 1,605[c]			1,620	3,068			
$[CoL(ac)_2]$	1,585[a] 1,543[b] 1,596[c]	1,588	1,367	1,606	3,042	2,919	455	515
$[NiL(ac)_2]$	1,595[a] 1,545[b] 1,598[c]	1,579	1,372	1,617	3,048	2,910	410	545
$[CuL(ac)_2]$	1,612[a] 1,555[b] 1,602[c]	1,594	1,378	1,603	3,055	2,920	430	536
$[CuL(acac)_2]$	1,610[a] 1,560[b] 1,601[c]			1,605	3,060	2,925	435	509
$[CuL(fms)_2]$	1,615[a] 1,559[b] 1,600[c]			1,611	3,053	2,909	425	543

Note: (a) azomethine, (b) pyridinecarboxaldehyde, and (c) 2,6-diamino-4-phenyl-1,3,5-triazine ring ν(C=N) bands.

Table 3: Electronic spectral and magnetic moment data of metal complexes

Compounds	Magnetic moment (B.M)	Spectral bands (cm^{-1})	Assignments	Δ_o (cm^{-1})	B^a (cm^{-1})	β	Geometry
L		26,315	n–π*/π–π*				
		38,461	π–π*				
$[CoL(ac)_2]$	3.75	16,077	$^4T_{1g} \rightarrow {}^4A_{2g(F)}$	12098.1	864.15	0.771	Oh
		34,482	$^4T_{1g} \rightarrow {}^4T_{1g(p)}$				
$[NiL(ac)_2]$	2.76	15,015	$^3A_{2g(F)} \rightarrow {}^3T_{1g(F)}$	6606.6	600.6	0.556	Oh
		32,258	$^3A_{2g(F)} \rightarrow {}^3T_{1g(p)}$				
$[CuL(ac)_2]$	1.68	15,625	$^2B_{1g} \rightarrow {}^2E_g$				SP
		34,502	$^2B_{1g} \rightarrow {}^2A_{1g}$				
$[CuL(acac)_2]$	1.77	15,503	$^2E_g \rightarrow {}^2T_{2g}$				Oh
$[CuL(fms)_2]$	1.43	15,105	$^2B_{1g} \rightarrow {}^2E_g$				SP
		33,898	$^2B_{1g} \rightarrow {}^2A_{1g}$				

[a] *B* values used for Co(II) 1,120 and Ni(II) 1,080 cm^{-1}

which support octahedral geometry. Dark green $[CuL(ac)_2]$ shows spectral bands at 15,625 and 34,502 cm^{-1} assigned to $^2B_{1g} \rightarrow {}^2E_g$ and $^2B_{1g} \rightarrow {}^2A_{1g}$, respectively, indicative of square planar geometry (Figure 1c). Green $[CuL(fmc)_2]$ shows spectral bands at 15,105 and 33,898 cm^{-1} assigned to $^2B_{1g} \rightarrow {}^2E_g$ and $^2B_{1g} \rightarrow {}^2A_{1g}$, respectively, indicative of square planar geometry (Figure 1d). The spectrum of $[CuL(acac)_2]$ displays a

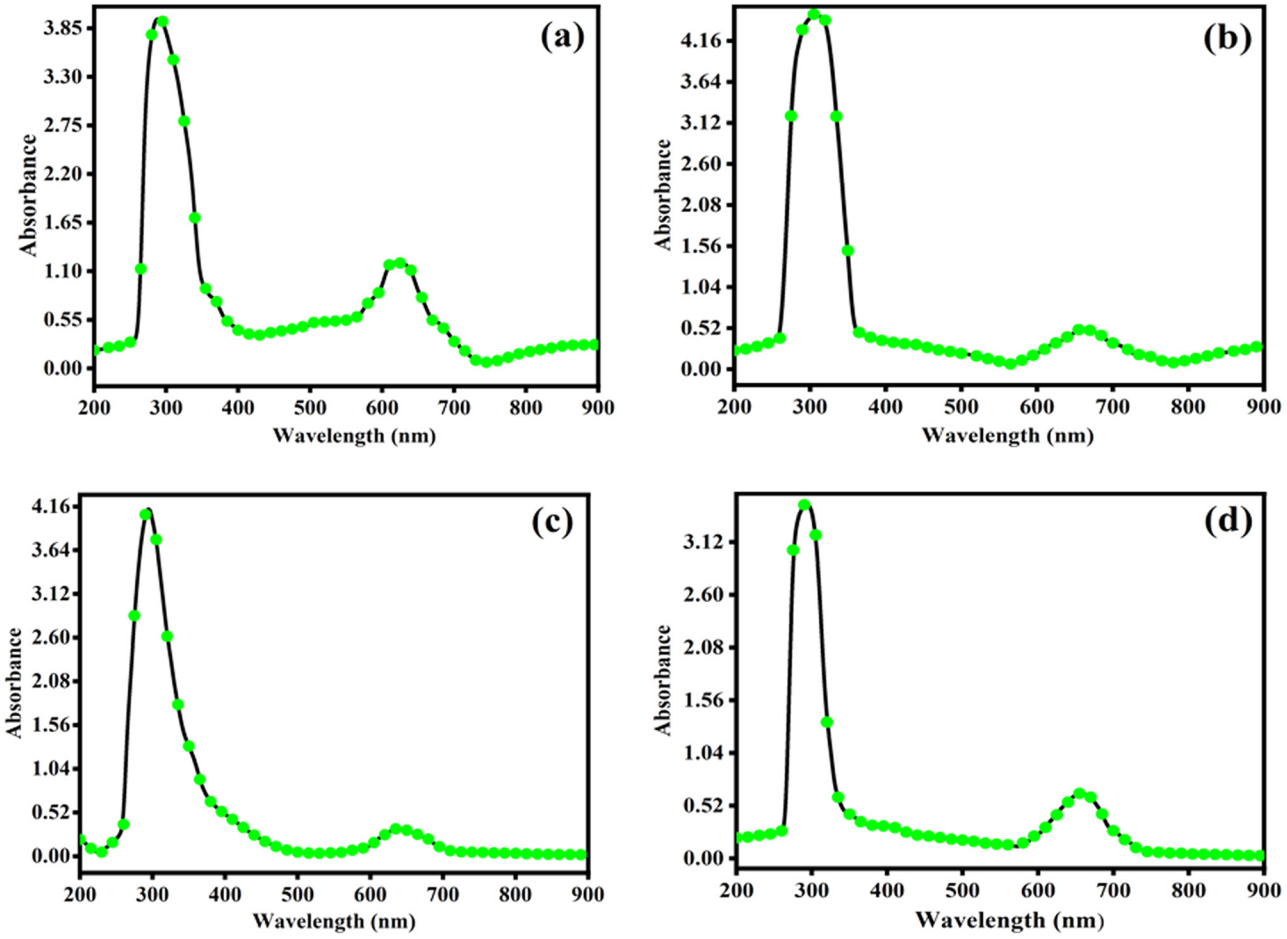

Figure 1: Electronic spectra of (a) $[CoL(ac)_2]$, (b) $[NiL(ac)_2]$, (c) $[CuL(ac)_2]$, and (d) $[CuL(fms)_2]$ metal complexes.

broad band at 15,503 cm^{-1}, which is consistent with the expected octahedral geometry, which corresponds to the $^2E_g \rightarrow {}^2T_{2g}$ transition [26]. These Cu(II) complexes exhibited a magnetic moment value very close to the spin value for an unpaired between 1.73 and 178 B.M.

3.4 Thermogravimetric study

To make certain the proposed formula of compounds, thermal degradation patterns were investigated under nitrogen flow. The simultaneous TG-DTG curves are shown in Figure 2 and temperature ranges, mass losses, residues, and maximum decomposition steps are listed in Table 4. The total mass losses from the TG curves are found to be 63.09% for L, 85.14% for $[CoL(ac)_2]$, 84.58% for $[NiL(ac)_2]$, 77.27% for $[CuL(ac)_2]$, 74.28% for $[CuL(acac)_2]$, and 82.78% for $[CuL(fms)_2]$. The TG curves showed that the thermal decomposition of ligand takes place in one step, while the metal complexes undergo two to five decomposition steps eliminating different fragments in the temperature range of 50–800°C, confirmed by the DTG curves. The decomposition pattern of metal complexes indicates the detachment of chelates and leaving respective metal oxides at final temperature. It was observed that the attached anionic groups in metal salts, electronegativity, and atomic radius of metals influenced thermal stability and pattern of the decomposition process [27].

The anhydrous ligand shows thermal stability up to 200°C and then degrades until it reaches 525°C, which is accompanied by a 57.73% mass loss, leaving more than 35% residue (Figure 2a). This step corresponds to the loss of two 2-pyridinecarboxaldehyde moieties. The first step occurs at a maximum temperature of 396.60°C.

The TG-DTG thermograms for Co(II) and Ni(II) complexes undergo a three-step decomposition (Figures 2b and c). The first stage of degradation occurred between 50 and 250°C in Co(II) and Ni(II) complexes, which are accompanied by mass losses of 4.28% and 28.17%, respectively. This step corresponds to the loss of moisture in Co(II) and triazine moieties in Ni(II) complexes. The first decomposition step occurred at maximum temperatures of 112.62°C and 208.32°C. The second decomposition step occurred between 250 and 360°C, which are associated with 23.27% for Co(II) and 23.08% for Ni(II) complexes due to the loss of acetate groups. The second decomposition step occurs at maximum temperatures of 305.82°C and 283.56°C. The

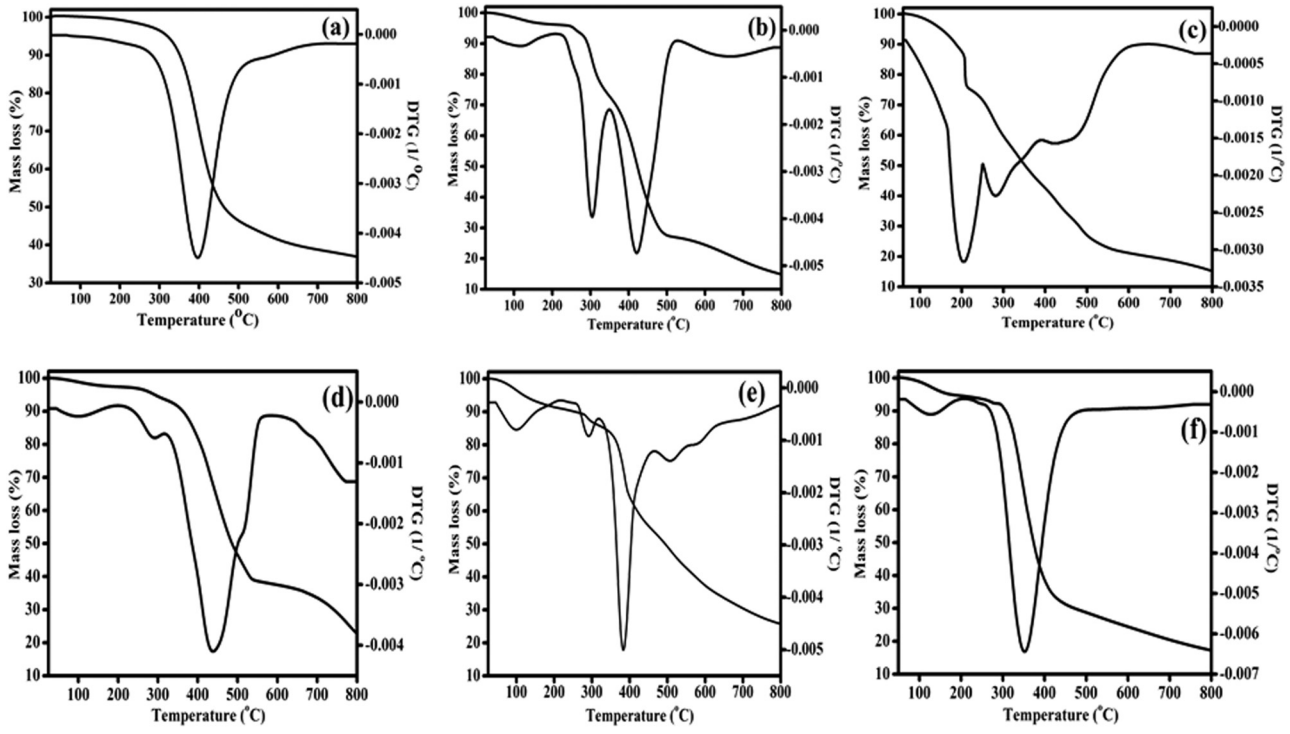

Figure 2: Simultaneous TG-DTG thermograms of (a) L, (b) $[CoL(ac)_2]$, (c) $[NiL(ac)_2]$, (d) $[CuL(ac)_2]$, (e) $[CuL(acac)_2]$, and (f) $[CuL(fms)_2]$ complexes in nitrogen atmosphere.

Table 4: Thermoanalytical (TG-DTG) data of the ligand and its metal complexes

Compound	Step	Temp. range (°C)	Mass loss (%)	DTG_{max} (°C)	DTG_{max} (%)	Total mass loss (%)	Residue (%)
L	I	200–525	57.73	396.6	29.33	63.09	36.91
$[CoL(ac)_2]$	I	50–250	4.28	112.62	2.38	85.14	14.86
	II	250–360	23.27	305.82	17.34		
	III	360–565	45.41	422.21	48.96		
$[NiL(ac)_2]$	I	50–250	28.17	208.32	13.54	84.58	15.42
	II	250–360	23.08	283.56	36.96		
	III	360–600	27.6	458.06	66.32		
$[CuL(ac)_2]$	I	50–225	2.62	102.35	1.57	77.27	22.73
	II	225–325	4.04	292.23	5.21		
	III	325–565	54.95	441.11	33.04		
$[CuL(acac)_2]$	I	50–200	9.23	87.04	3.23	74.28	25.72
	II	200–335	6.5	290.45	12.27		
	III	335–415	23.98	384.59	27.28		
	IV	415–555	18.8	509.46	52.08		
	V	455–665	9.52	583.13	61.09		
$[CuL(fms)_2]$	I	50–180	4.88	125.86	2.85	82.78	17.22
	II	180–445	62.98	351.67	35.91		

third decomposition step within the ranges of 360–565°C in Co(II) and 360–600°C in Ni(II) complexes is accompanied by mass losses of 45.41% and 27.6%, which are assigned to the loss of $C_{12}H_{10}N_2$ and C_6H_5N as evolved components. The third decomposition step occurs at maximum temperatures of 422.21 and 458.06°C.

In contrast to Co(II) and Ni(II) complexes, Cu(II) complexes showed multiple decompositions at various temperature ranges due to the nature of coordinated groups. $[CuL(ac)_2]$, $[CuL(acac)_2]$, and $[CuL(fms)_2]$ showed three, five, and two successive steps of decomposition, respectively. The thermal degradation of the $[CuL(ac)_2]$ occurs mainly in three degradation stages (Figure 2d). The first stage of degradation occurred between 50 and 225°C, which is accompanied by a mass loss of 2.62%. This step corresponds to the loss of methanol solvent. The first step of decomposition occurs at a maximum temperature of 102.35°C. The second major step of mass loss between 225 and 325°C corresponds to the loss of carbon monoxide (CO) gas. The second step of decomposition occurs at a maximum temperature of 292.23°C. In the third major step, triazine and acetate groups were evolved in the temperature range of 325–565°C with a 54.95% weight loss, leaving CuO as a residue. The third step of decomposition occurs at a maximum temperature of 441.11°C. The thermal degradation of the $[CuL(acac)_2]$ occurs in five degradation stages (Figure 3e). The first stage of degradation occurred between 50 and 200°C and shows a mass loss of 8.23% and T_{max} of 87.04°C, corresponding to the degradation. This step corresponds to the loss of the C_3H_4O component. The second step of mass loss occurred between 200 and 335°C, which is accompanied by a mass loss of 6.50% and T_{max} of 290.45°C, corresponding to the loss of CO_2 gas. The third major step of mass loss occurred between 335 and 415°C, which is accompanied by a mass loss of 23.98% and T_{max} of 384.59°C, corresponding to the loss of triazine moiety. The last two minor steps correspond to decompositions of 2-pyridinecarboxaldehyde and the residual ligand. $[CuL(fms)_2]$ shows a two-step degradation (Figure 3f). In the first step, 4.88% was observed between 50 and 180°C with the evolution of SO_x gas. The first step of decomposition occurs at a maximum temperature of 125.86°C. The second major step occurred between 180 and 445°C resulting in a 62.98% mass loss. This step corresponds to the elimination of ligand and leaving bluish black CuS as a residue. The second decomposition stage occurs at a maximum temperature of 351.67°C.

3.5 Thermal kinetics investigation

Non-isothermal methods have been widely applied for the calculation of kinetic parameters of solid-state decomposition reactions by the thermal technique (TG-DTG). The decomposition rate is the product of two separate functions: temperature and conversion, which are represented by the following mathematical equation:

$$v = \left(\frac{d\alpha}{dt}\right) = k(T)f(\alpha) = A\exp\left(\frac{-E_a}{RT}\right)f(\alpha) \qquad (1)$$

where α is the fraction decomposed at time t, $f(\alpha)$ is a temperature-independent function of conversion whose

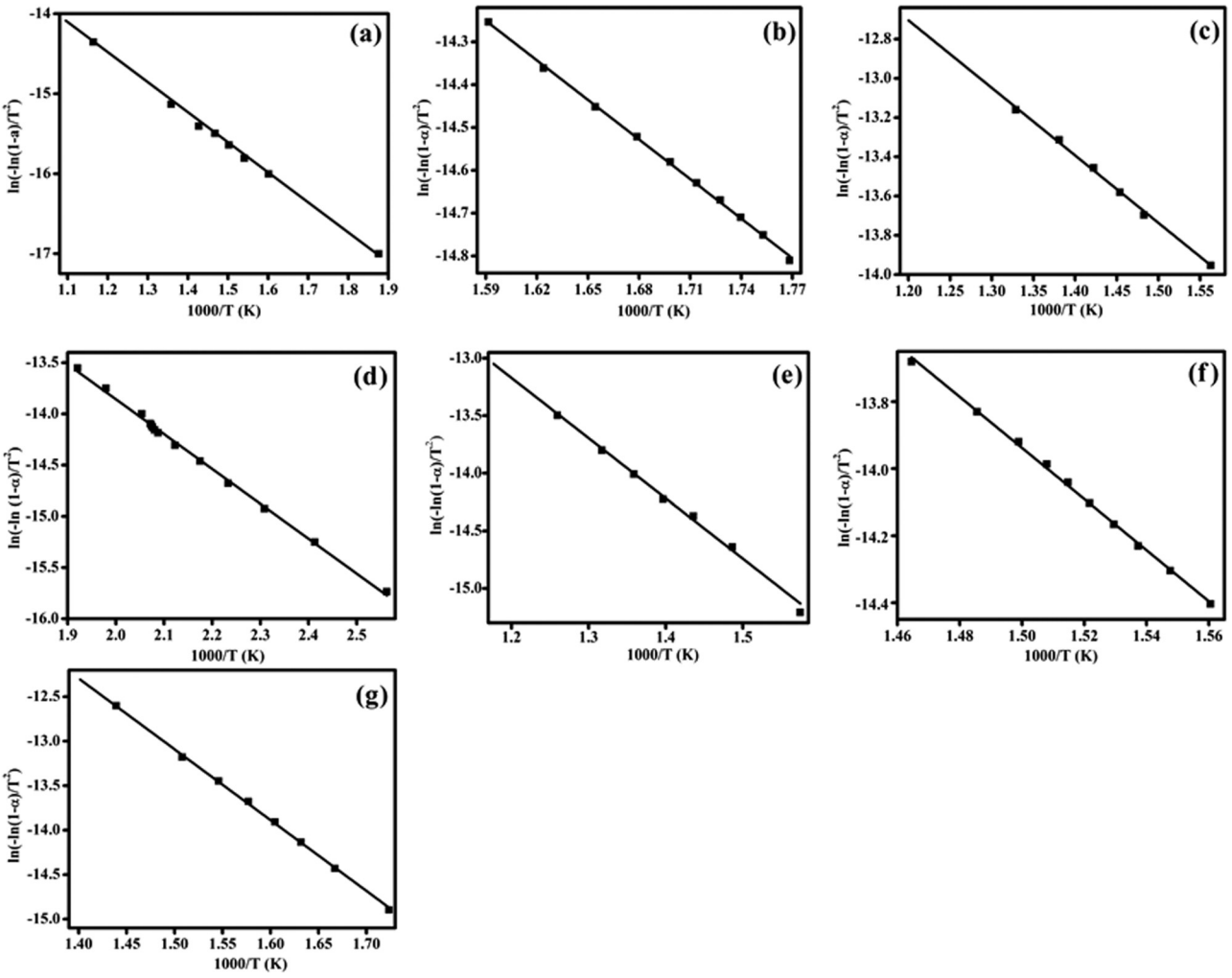

Figure 3: Coats–Redfern plots for major decomposition of (a) L, (b) [CoL(ac)$_2$, II step], (c) [CoL(ac)$_2$, III step], (d) [NiL(ac)$_2$], (e) [CuL(ac)$_2$], (f) [CuL(acac)$_2$], and (g) [CuL(fms)$_2$] complexes.

function is dependent on the mechanism of decomposition, $k(T)$ is a temperature-dependent function, A is the frequency factor, assumed to be independent of temperature, E_a is the apparent activation energy, T is the absolute temperature, and R is the gas constant (8.314 J/mol K). In case of non-isothermal conditions, the linear heating rate of $\beta = dT/dt$, equation (1) can be written as:

$$\left(\frac{d\alpha}{dT}\right) = \left(\frac{A}{\beta}\right) f(\alpha) \exp\left(\frac{(-E_a)}{RT}\right) \tag{2}$$

After the integration and approximation, equation (2) can be represented by

$$g(\alpha) = -\frac{E_a}{RT} + \ln\left[\frac{AR}{\beta E_a}\right] \tag{3}$$

where $g(\alpha)$ is a function of α dependent on the mechanism of reaction. This is a basic equation for the evolution of kinetic parameters. The integral on the right-hand side is known as the temperature integral and it has no closed-form solution. Herein, kinetic information has been assessed using the Coats–Redfern method [28] and shows the best linearity of data. It can be represented as:

$$g(\alpha) = \int_0^{\alpha} d(\alpha)/f(\alpha) = \left(\frac{A}{\beta}\right) \int_{T_0}^{T} \exp\left(\frac{-E_a}{RT}\right) dT \tag{4}$$

where T_0 is the onset temperature. No conversion occurs before T_0, therefore, T_0 can be set equal to zero for convenience. This equation on integration gives:

$$\ln\left[-\frac{\ln(1-\alpha)}{T^2}\right] = -\frac{E_a}{RT} + \ln\left[\frac{AR}{\beta E_a}\right] \tag{5}$$

Table 5: Thermal kinetic parameters of the ligand and its metal complexes

Compound	Stage	E (kJ mol^{-1})	ln A (min^{-1})	ΔH (kJmol^{-1})	ΔS (kJmol^{-1}K^{-1})	ΔG (kJ)	r^2
L	I	30.886	1.147	27.588	−0.237	121.87	0.998
[CoL(ac)$_2$]	I	10.416	−2.748	9.480	−0.259	38.724	0.994
	II	25.595	1.672	23.058	−0.231	93.765	0.999
	III	28.583	2.559	25.073	−0.226	120.71	0.998
[NiL(ac)$_2$]	I	28.294	4.070	26.562	−0.208	69.899	0.997
	II	9.974	−1.218	7.617	−0.254	79.818	0.997
	III	6.694	−2.302	2.885	−0.267	125.476	0.998
[CuL(ac)$_2$]	I	3.040	−6.377	2.189	−0.289	31.773	0.999
	II	19.212	−0.845	16.782	−0.251	90.360	0.997
	III	43.523.	4.669	39.856	−0.209	132.20	0.995
[CuL(acac)$_2$]	I	13.992	0.474	13.268	−0.238	34.037	0.998
	II	5.733	−3.955	3.319	−0.277	83.942	1
	III	63.395	9.434	60.197	−0.168	125.036	0.998
	IV	5.506	−3.287	1.270	−0.276	142.239	0.999
	V	9.105	−2.302	4.257	−0.269	4.526	0.997
[CuL(fms)$_2$]	I	6.126	−4.290	5.079	−0.273	39.491	0.998
	II	66.181	10.827	63.257	−0.156	118.22	0.999

A plot of the left-hand side against 1,000/T was drawn. The E_a values were calculated from the slope and A values from the intercept. The other thermodynamic parameters of the decomposition reaction, such as enthalpy (ΔH), entropy (ΔS), and Gibbs free energy (ΔG), were calculated using the following equations:

$$\Delta H = E_a - RT \tag{6}$$

$$\Delta S = R[\ln(Ah/kT)] \tag{7}$$

$$\Delta G = \Delta H - T\Delta S \tag{8}$$

where k is Boltzmann's constant, h is Planck's constant, and T is the DTG peak temperature. The decomposition reactions are classified as exothermic ($\Delta H < 0$ or $\Delta G < 0$) and/or endothermic ($\Delta H > 0$ or $\Delta G > 0$) on the basis of whether they give off or absorb heat energy. The reaction for which ΔG is positive and ΔS is negative is considered as unfavorable or non-spontaneous slow decomposition reaction. The kinetic parameters are listed in Table 5 and linearization curves of major decomposition stage of synthesized compounds are shown in Figure 3(a–g). The linear correlation coefficients (r^2) of thermal decomposition steps were found to lie in the range of 0.99–1, showing a good fit with the linear function.

From the results, it has been observed that all decomposition steps exhibited a straight line using the method of Coats–Redfern to plot the left-hand side vs 1,000/T and suggesting first-order and endothermic reaction because of the positive values of enthalpy and Gibbs free energy. Taking the major decomposition stage as a criterion, the data show that E_a for metal complexes are higher values than other degradation stages, indicating that the rate of decomposition for this stage is difficult and proceeding through high endothermic stages than other stages. The activation energy in terms of thermal stability of Co(II), Ni(II), and Cu(II) complexes is expected to increase in relation with decreasing their radius [29], the smaller size of Cu(II) permits a closer approach of the ligand, as compared to Co(II) and Ni(II). Hence, the E_a value for Cu(II) complexes is higher than that of others, that is, thermal stability of Cu(II) complexes is higher than that of others. The values of entropies are negative for all of the compounds, which indicate that the decomposition reactions are slower than normal and activated complexes have a more ordered structure (non-spontaneously) than reactants.

4 Conclusions

The Schiff-base ligand was synthesized via condensation of 2-pyridinecarboxaldehyde and 2,6-diamino-4-phenyl-1,3,5-triazine. The metal complexes of the prepared ligand were synthesized with Co(II), Ni(II), and Cu(II) salts. The observed result indicates that the synthesized metal complexes show an octahedral and square planar geometry. The decomposition process of all complexes occurs in multi-steps and the ligand undergoes a one-step decomposition, and thermal degradation reactions follow first-order reactions. In all metal complexes, the activation energy for the major step is greater than those

of the other minor steps. The entropy of all compounds was negative, whereas enthalpy and Gibbs free energy were positive for all compounds. We also conclude that Cu(II) complexes are more stable than other synthesized metal complexes.

Acknowledgments: The authors are grateful to the Researchers Supporting Project number (RSP-2020/113), King Saud University, Riyadh, Saudi Arabia for the support.

Conflict of interest: Authors declare no conflict of interest.

References

[1] Karakoç M, Dede B, Erdem-Tunçmen M, Karipcin F. Synthesis, characterization, DFT calculations and catalase-like enzymatic activities of novel hexadentate Schiff base and its manganese complexes. J Mol Struct. 2019;1186:250–62.

[2] Warad I, Ali O, Ali AA, Jaradat NA, Hussein F, Abdallah L, et al. Synthesis and spectral Identification of three Schiff bases with a 2-(piperazin-1-yl)-*N*-(thiophen-2-yl methylene) ethanamine moiety acting as novel pancreatic lipase inhibitors: Thermal, DFT, antioxidant, antibacterial, and molecular docking investigations. Molecules. 2020;25:2253. doi: 10.3390/molecules25092253.

[3] Gesawat AA, Shakeel F. Synthesis and characterization of ternary complexes of chromium(III) with l-histidine and various diols. Arab J Chem. 2017;10:S2575–9.

[4] Zoubi WA, Mohamed SG, Al-Hamdani AAS, Mahendradhanya AP, Ko YG. Acyclic and cyclic imines and their metal complexes: recent progress in biomaterials and corrosion applications. RSC Adv. 2018;8:23294–318.

[5] Görgülü G. Experimental and theoretical study of a novel naphthoquinone Schiff base. Open Chem. 2018;16:1115–21.

[6] Kalofolias DA, Weselski M, Siczek M, Lis T, Tsipis AC, Tangoulis V, et al. Dinuclear and mononuclear rhenium coordination compounds upon employment of a schiff-base triol ligand: structural, magnetic, and computational Studies. Inorg Chem. 2019;58(13):8596–606.

[7] Liu Y, Deng W, Meng Z, Wong WY. A tetrakis(terpyridine) ligand–based cobalt(II) complex nanosheet as a stable dual-ion battery cathode material. Small. 2020;16(17):1905204.

[8] Miloud MM, El-ajaily MM, Al-noor TH, Al-barki NS. Antifungal activity of some mixed ligand complexes incorporating Schiff bases. J Bacteriol Mycol. 2020;7(1):1122.

[9] Verma AM, Kishore N. Kinetics of decomposition reactions of acetic acid using DFT approach, the open. Chem Eng J. 2018;12:14–23.

[10] Khan MY, So S, Silva GD. Decomposition kinetics of perfluorinated sulfonic acids. Chemosphere. 2020;238: 124615.

[11] Nugent J, Shire BR, Caputo DFJ, Pickford HD, Nightingale F, Houlsby ITT, et al. Synthesis of all-carbon disubstituted bicyclo[1.1.1]pentanes by iron-catalyzed Kumada cross-coupling. Chem An Asian J. 2020;59(29):11866–70.

[12] Yang C, Ju T, Wang X, Ji Y, Yang C, Lv H, et al. The preparation of a novel iron/manganese binary oxide for the efficient removal of hexavalent chromium [Cr(VI)] from aqueous solutions. RSC Adv. 2020;10:10612–23.

[13] Buldurun K, Turan N, Bursal E, Mantarcı A, Turkan F, Taslimi P, et al. Synthesis, spectroscopic properties, crystal structures, antioxidant activities and enzyme inhibition determination of Co(II) and Fe(II) complexes of Schiff base. Res Chem Intermed. 2020;46:283–297.

[14] Subodh, Prakash K, Masram DT. Chromogenic covalent organic polymer-based microspheres as solid-state gas sensor. J Mater Chem C. 2020;8:9201–4.

[15] Boepple M, Zhu Z, Hu X, Udo W, Barsan N. Impact of heterostructures on hydrogen sulfide sensing: Example of core-shell $CuO/CuFe_2O_4$ nanostructures. Sens Actuators B. 2020;321:128523.

[16] Rambabu A, Kumar MP, Ganji N, Daravath S, Shivaraj. DNA binding and cleavage, cytotoxicityand antimicrobial studies of Co(II), Ni(II),Cu(II) and Zn(II) complexes of 1-((*E*)-(4-(trifluoromethoxy)phenylimino)methyl)naphthalen-2-ol Schiff base. J Biomol Struct Dyn. 2020;38(1):307–31.

[17] Sarango-Ramírez MK, Lim DW, Kolokolov DI, Khudozhitkov AE, Stepanov AG, Kitagawa H. Superprotonic conductivity in metal–organic framework via solvent-free coordinative urea insertion. J Am Chem Soc 2020;142(15):6861–5.

[18] Jeyaraman P, Alagarraj A, Natarajan R. In silico and in vitro studies of transition metal complexes derived from curcumin–isoniazid Schiff base. J Biomol Struct Dyn. 2019;38(2):488–99.

[19] Mandal U, Mandal S, Chakraborty B, Rizzoli C, Bandyopadhyay D Synthesis and crystal structure of some first row transition metals containing a common Schiff base. Polyhedron. 2020;177:114320.

[20] Burns DT, Walker MJ. Origins of the method of standard additions and of the use of an internal standard in quantitative instrumental chemical analyses. Anal Bioanal Chem. 2019;411:2749–53.

[21] Pavlov VA, Shushenachev YV, Zlotin SG. Possible physical basis of mirror symmetry effectin racemic mixtures of enantiomers: From Wallach'sRule, non linear effects, B–Z DNA transition,and similar phenomena to mirror symmetry effectsof chiral objects. Symmetry. 2020;12:889. doi: 10.3390/sym12060889.

[22] Gutiérrez-Serpa A, Napolitano-Tabares PI, Šulc J, Pacheco-Fernández I, Pino V. Role of ionic liquids in composites in analyticalsample preparation. Separations. 2020;7:37. doi: 10.3390/separations7030037.

[23] Maleki A, Niksefat M, Rahimi J, Azadegan S. Facile synthesis of tetrazolo[1,5-*a*]pyrimidine with the aid of an effective gallic acid nanomagnetic catalyst. Polyhedron. 2019;167:103–110.

[24] Kang MS, Cho J, Nayab S, Jeong JH. Synthesis and characterization of Zn(II) and Cu(II) complexes bearing (chiral substituent)(diethyl)-ethanediamine derivatives as precatalysts for rac-lactide polymerization. Polyhedron. 2019;158:135–43.

[25] Cirri A, Hernández HM, Johnson CJ High precision electronic spectroscopy of ligand-protected gold nanoclusters: effects of composition, environment, and ligand chemistry. J Phys Chem A. 2020;124(8):1467–79.
[26] Sevgi F, Bagkesici U, Kursunlu AN, Guler E. Fe(III), Co(II), Ni(II), Cu(II) and Zn(II) complexes of Schiff bases based-on glycine and phenylalanine: Synthesis, magnetic/thermal properties and antimicrobial activity. J Mol Struct. 2018;1154:256–60.
[27] Kavith N, Lakshmi PVA. Synthesis, characterization and thermogravimetric analysis of Co(II), Ni(II), Cu(II) and Zn(II) complexes supported by ONNO tetradentate Schiff base ligand derived from hydrazino benzoxazine. J Saudi Chem Soc. 2017;21(1):S457–66.
[28] Singh A, Singh S, Soni PK, Mukherjee N. Non-isothermal thermogravimetric degradationkinetics, reaction models and thermodynamic parameters of vinylidene fluoride based fluorinated polymers. J Macromol Science, Part B. 2019;59(1):1–24.
[29] Al-Rasheed HH, Mohammady SZ, Dahlous K, Siddiqui MRH, El-Faham A. Synthesis, characterization, thermal stability and kinetics of thermal degradation of novel polymers based-s-triazine Schiff base. J Polym Res. 2020;27:10.